Transverse and longitudinal resolution of the synthetic aperture focusing technique

R.N. THOMSON

This paper derives expressions that determine both the transverse and longitudinal resolution of the SAFT process whilst taking into account the pulsed nature of the ultrasound used in the process. Some experimental results supporting the theoretical results are also presented.

KEYWORDS: ultrasonic testing, synthetic aperture focusing, resolution

Introduction

Despite recent developments in equipment, ultrasonic examination of a component still relies largely on the skilled operator to interpret the signals produced. Although replacement of the operator is not yet a possibility, he could be given more assistance in sizing and characterizing defects if equipment and techniques could be developed which would utilize more of the information contained in the reflected ultrasonic pulse.

One such technique that is claimed to have a resolution of the order of a wavelength is the synthetic aperture focusing technique (SAFT). This offers the possibility of sizing, in the field of ultrasonic non-destructive testing, to about 2 mm. To date the only theoretical verification of this resolution is based on a calculation of the transverse resolution using continuous wave theory[1]. Since SAFT uses pulsed ultrasound to construct an image, the use of continuous wave theory to calculate resolutions might lead to erroneous results. In the following, expressions are derived for both the transverse and longitudinal resolutions whilst taking into account the pulsed nature of the ultrasound. The results of the theoretical treatment are then compared with a limited number of experiments.

A review and exact description of SAFT

The concept of synthetic aperture focusing dates back to the early 1950s[4] when it was used for high-resolution all-weather terrain imaging by radar. The first application of the method to ultrasonics met with limited success due to the elaborate optical processing that was used[5]. However, rapid developments in digital computing in the '70s made it possible to avoid the difficulties of optical processing and apply the principles of SAFT to digitized ultrasonic signals. Much work on digital SAFT has been done at the University of Michigan[2] using a laboratory-based system.

The author is in the Scientific Services Department, CEGB, Beckwith Knowle, Otley Road, Harrogate, North Yorkshire, UK. Paper received 7 March 1983.

The SAFT can be described in mathematical terms with reference to Fig. 1. To determine the image $I(r'_j)$ at the point r'_j the time taken for the ultrasound to traverse the distance $|r_{si} - r'_j|$ denoted by t_{ij} is calculated for each received signal position r_{si}. The set of values of received signals $S(r_{si}, t_{ij})$ are then summed to determine $I(r'_j)$. Therefore if the point r'_j is associated with a reflector a coherent summation will occur resulting in a large value of I; if this point is not associated with such a reflector no coherent summation will occur, resulting in a small value for I.

Expressed more precisely, the SAFT image field is $I(r')$ where

$$I(r'_j) = 1/n \sum_{i=1}^{n} S(r_{si}, t_{ij})$$

and

$$t_{ij} = 2/c|r_{si} - r'_j|$$

where n is the number of signals in the aperture and c the velocity of ultrasound in the medium.

It will be shown in the following that the best achievable resolution of SAFT is $A/4$ in the transverse direction, and $L/4$ in the longitudinal direction where A

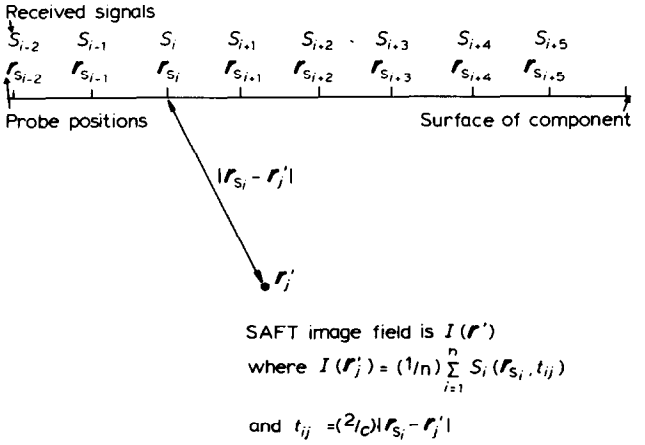

Fig. 1 Parameters involved in the calculation of the SAFT image field amplitude

0041-624X/84/010009-07/$03.00

is the ultrasonic probe's crystal width and L is the pulse length.

The relationship between the SAFT image and the reflector distribution

Before determining the resolution of the SAFT procedure it is important to define how the image depends on the reflectors present in the component under investigation. The equation that describes this relationship contains the point spread function for SAFT which is investigated in detail to determine resolutions. The time dependent Kirchoff scalar wave theory in the Fraunhofer far-field region is used to determine this relationship.

The starting point is the scalar wave equation

$$\nabla^2 P(r, t) + (1/c^2)\,\frac{\partial^2 P(r, t)}{\partial t^2} = F(r, t) \qquad (1)$$

which is obeyed by the ultrasonic pressure field $P(r, t)$ in the material being investigated; $F(r, t)$ represents the distribution of sources in the material and c is the velocity of the ultrasound (mode conversions are being ignored).

A general integral solution to (1) can be obtained[3] and written

$$P(r, t) = -(1/4)\pi \int_v \frac{d^3 r' F(r, t-1/c\,|r-r'|)}{|r-r'|} \qquad (2)$$

Equation (2) relates the pressure at r and t, $P(r, t)$, to the distribution of sources in the material $F(r, t)$. If there is only one point source such as a piezoelectric transmitter at r_s on the surface of the material being investigated, generating a pulse of the form $f(r, t)\exp(i\omega t)$, then (2) is reduced to

$$P(r, t) = -(1/4)\,\pi\,\frac{f(r_s, t-1/c\,|r-r_s|)\exp(i\omega[t-1/c|r-r_s|])}{|r-r_s|} \qquad (3)$$

This is the primary field set up by the transmitter and is denoted by $P_1(r, t)$ in the analysis below.

If the material has a distribution of reflection coefficients described by $R(r)$ then this distribution will perturb the primary field set up by the transmitter in (3), that is, a secondary set of sources will be created described by $R(r)P_1(r, t)$. These secondary sources will give rise to a secondary field $P_2(r, t)$ described by (using (2) and (3))

$$P_2(r, t) = -(1/4)\pi \int_v \frac{d^3 r' R(r') f(r_s, t-T)\exp(i\omega[t-T])}{|r'-r_s|\,|r-r'|} \qquad (4)$$

where $T = (1/c)(|r' - r_s| - |r - r'|)$ and the total field can be written as

$$P(r, t) = P_1(r, t) + P_2(r, t) \qquad (5)$$

The above argument can be used again to generate tertiary and higher-order sources (re-echoes), however, these are assumed to give a negligible contribution to the total field and are therefore neglected.

In single-transducer ultrasonic pulse-echo systems it is $P(r, t)$ at r_s that is measured where r_s is the position of both the transmitter and receiver, that is $P(r_s, t)$ is measured. Further, if we only consider times $t > t_T$ where t_T is the length of time the transmitter pulse envelope is non-zero, then from (3)-(5),

$$P(r_s, t) = -(1/4)\pi \int \frac{d^3 r' R(r') f(r_s, t-T)\exp(i\omega[t-T])}{|r_s - r'|^2} \qquad (6)$$

for $t > t_T$ and $T = (2/c)\,|r_s - r'|$.

Equation (6) expresses how the received field at r_s, $P(r_s, t)$, is related to the transmitter pulse, $f(r_s, t)\exp(i\omega t)$ and the distribution of reflection coefficients in the material $R(r)$. By applying the SAFT process described in the previous section to the received signals described in (6) an expression can be obtained which relates the SAFT image to the distribution of reflection coefficients as is shown below.

It was defined above that the SAFT process is described by

$$I(r'_j) = (1/n) \sum_{i=1}^{n} S(r_{si}, t_{ij})$$

where $t_{ij} = (2/c)\,|r_{si} - r'_j|$. The continuous form of the above equation is described by

$$I(r'') = \int_{\text{surface}} S(r_s, t = 2/c\,|r_s - r''|)\,dr^2_s \qquad (7)$$

The continuous and discrete descriptions both produce the same image provided the effects of sampling in the discrete case are fully taken into account. If the image width of interest is of the order of the depth of imaging then a sample spacing of $ds = |r_{si-1} - r_{si}| = \lambda/2$ in the discrete case ensures that sampling effects are not seen. With the above restriction imposed the continuous description is used in the following, for analytical ease.

Substituting (6) into (7) and noting that $f(r, t)\exp(i\omega t)$ is usually independent of r (that is, the same transmitter pulse is generated at each probe position) then

$$I(r'') = -(1/4)\,\pi \int_v d^3 r' R(r') X(r'', r', \omega/c) \qquad (8)$$

where

$$X(r'', r, \omega/c) = \int_{\text{Surface}} \frac{f(u)\exp(i\omega u)\,d^2 r_s}{|r_s - r'|^2} \qquad (9)$$

and

$$u = (2/c)\,(|r_s - r''\,| - |r_s - r'|)$$

When there is only one point reflector, that is, $R(r) = 4\pi\delta(r' - r)$, then $I(r'') = X(r'', r, \omega/c)$ where X is defined as the point spread function for SAFT. An investigation of X yields a measure of SAFT's resolution.

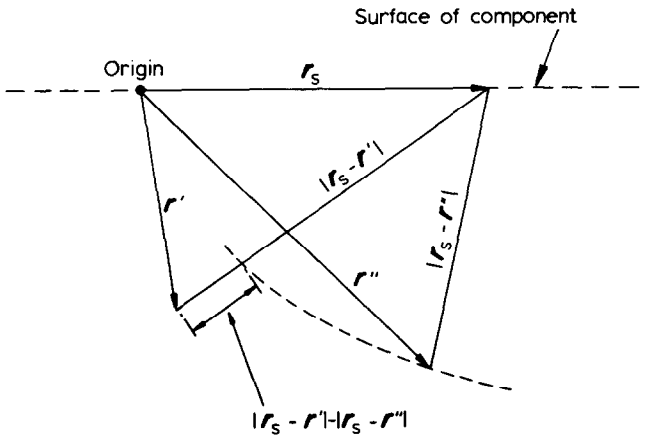

Fig. 2 Relationship between vectors used in theoretical treatment

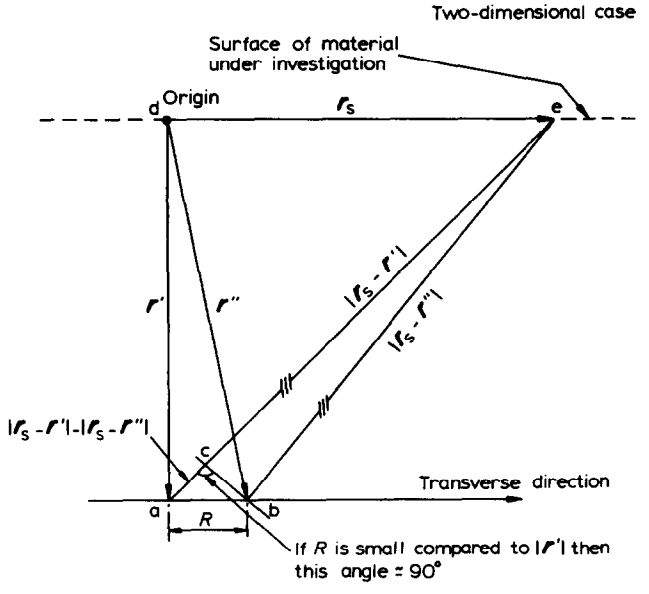

Fig. 3 Parameters involved in determining the transverse resolution of SAFT. The origin was chosen directly above the scattering point at r' for analysis ease

The resolution of SAFT

In the following only the two-dimensional case has been considered for simplicity, and therefore the surface integral in (9) was replaced by a line integral. A diagram of the various vectors and magnitudes involved in (9) is given in Fig. 2.

In the following the variation of X, with r' fixed and r'' moving parallel to the surface, was investigated to determine the transverse resolution, and with r' fixed with r'' moving away from r' normal to the surface, for longitudinal resolution.

Transverse resolution

A diagram of the various vectors and magnitudes involved in $X(r'', r', \omega/c)$ for this particular case is shown in Fig. 3. The origin of the coordinate system was chosen directly above the scattered source r' for analytical ease. From the diagram it can be seen that if R is a lot smaller than $|r'|$ then the angle acb is approximately equal to 90° and triangle ade is similar to triangle acb. Since these triangles are similar the following expression can be written

$$\frac{R}{|r_s - r'| - |r_s - r''|} = \frac{(|r'|^2 + r_s^2)^{1/2}}{|r_s|}$$

$$\text{So } |r_s - r'| - |r_s - r''| = \frac{Rr_s}{|r'|}\,(1 + r_s^2/|(r')^2|)$$

where r_s is the one-dimensional displacement of r_s on the surface of the material being investigated.

Now taking the Fraunhofer approximation and neglecting quadratic terms in $r_s/|r'|$ then

$$|r_s - r'| - |r_s - r''| = Rr_s/|r'| \tag{10}$$

Finally, substituting (10) into (9) the transverse variation of $X(r'', r', \omega/c)$, denoted by $X_T(R, |r'|, \omega/c)$ is given by

$$X_T(R, |r'|, \omega/c) = \int_{\text{Surface}} \frac{f(v)\exp(i\omega v)\,dr_s}{|r'|^2}$$

where

$$v = \frac{-2Rr_s}{c|r'|}$$

If the SAFT analysis is performed over a finite aperture, A, then the above expression can be written

$$X_T(R, |r'|, \omega/c) = \int_{-A/2}^{A/2} \frac{f(v)\exp(i\omega v)dr_s}{|r'|^2} \tag{11}$$

To evaluate the above expression further, the form of $f(t)$ has to be defined. The function $f(t)$ is chosen to have the following properties so that it represents, approximately, the envelope of a transmitter pulse

$$\begin{aligned} f(t) &= 0 \quad \text{for} \quad t > -p/2 \\ f(t) &= 1 \quad \text{for} \quad -p/2 < t < p/2 \\ f(t) &= 0 \quad \text{for} \quad t < p/2 \end{aligned} \tag{12}$$

Clearly p is the pulse duration.

It can be noted that the $f(v)$ term within (11) remains constant within the range of integration if

$$R \leqslant (c/2)\,(|r'|/A)\,p \tag{13}$$

Assuming R obeys the above inequality then (11) can be evaluated to yield the well-known diffraction function $\sin(x)/x$ which has its first zero when

$$R = \lambda|r'|/2A \tag{14}$$

Applying the Rayleigh resolution criterion[3] to this function yields the transverse resolution of the SAFT process, that is, $\lambda|r'|/2A$. However the above calculation is based on the constraints of (12)–(14), that is,

$$\lambda|r'|/2A \leqslant (c/2)\,(|r'|/A)\,P \tag{15}$$

which implies that $pc \geqslant \lambda$.

Hence if the pulse length is greater than the wavelength of the ultrasound being used, the transverse resolution of SAFT is given by (14). This condition on

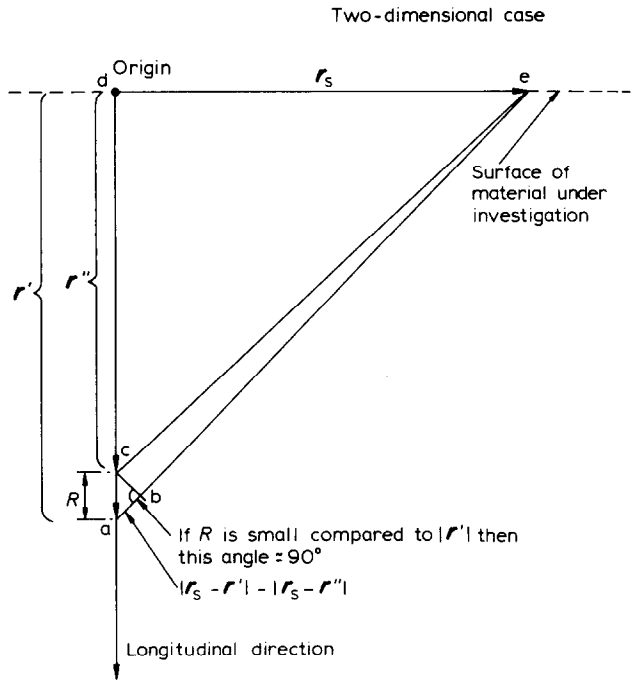

Fig. 4 Parameters involved in determining the longitudinal resolution of SAFT. The origin was chosen directly above the scattering point r' for analysis ease

the pulse length is very rarely not met by conventional ultrasonic probes.

Before finishing this discussion on the transverse resolution of SAFT a further restriction has to be taken into account. For a point reflector at r' the aperture A defined above should not exceed the beam spread at r' of the ultrasonic probe being used since no reflections and therefore no contributions to the integral in (11) occur at transducer positions in which the ultrasonic beam does not impinge on the point reflector. From standard ultrasonic transducer theory[6] the beam spread of an unfocused contact probe, in the far-field, at r', is given approximately by

$$\frac{2\lambda|r'|}{a} \qquad (16)$$

where a is the width of the crystal in the contact probe.

Thus the maximum value of A at depth $|r'|$ is given by (16), and feeding this value into (14) gives the best transverse resolution attainable with SAFT, and this equals $a/4$ where a is the transducer crystal width and the pulse length is greater than the wavelength.

Longitudinal resolution

A diagram of the various vectors and magnitudes involved in the point spread function $X(r'', r', \omega/c)$ for the longitudinal case is shown in Fig. 4. The origin of the coordinate system was chosen directly above the scattering source r' for analytical ease. From the diagram it can be seen that if R is a lot smaller than $|r'|$ then the angle abc is approximately equal to 90° and triangle abc is similar to triangle aed. Since these triangles are similar the following expression can be written

$$|r_s - r'| - |r_s - r''| = R(1 + r_s^2/|r'|^2)^{1/2}$$

Then using the same approximation as in the transverse case, that is, neglecting quadratic terms because $|r'| \gg r_s$, gives

$$|r_s - r'| - |r_s - r''| \simeq R$$

Hence the longitudinal variation of X, denoted by X_L is given by

$$X_L(R, |r'|, \omega/c) = \int_{\text{Surface}} \frac{f(y)\exp(i\omega y)\,dr_s}{|r'|^2} \qquad (17)$$

where $y = (2/c)R$ which implies

$$X_L(R, |r'|, \omega/c) = (A/|r'|^2) f(y) \exp(i\omega y)$$

So from (12)

$$X_L(R, |r'|, \omega/c) = 0$$

for $R \geq pc/4$

Therefore at longitudinal distances greater than $pc/4$ from the point scatterer the point spread function is zero. If the longitudinal resolution is defined as the

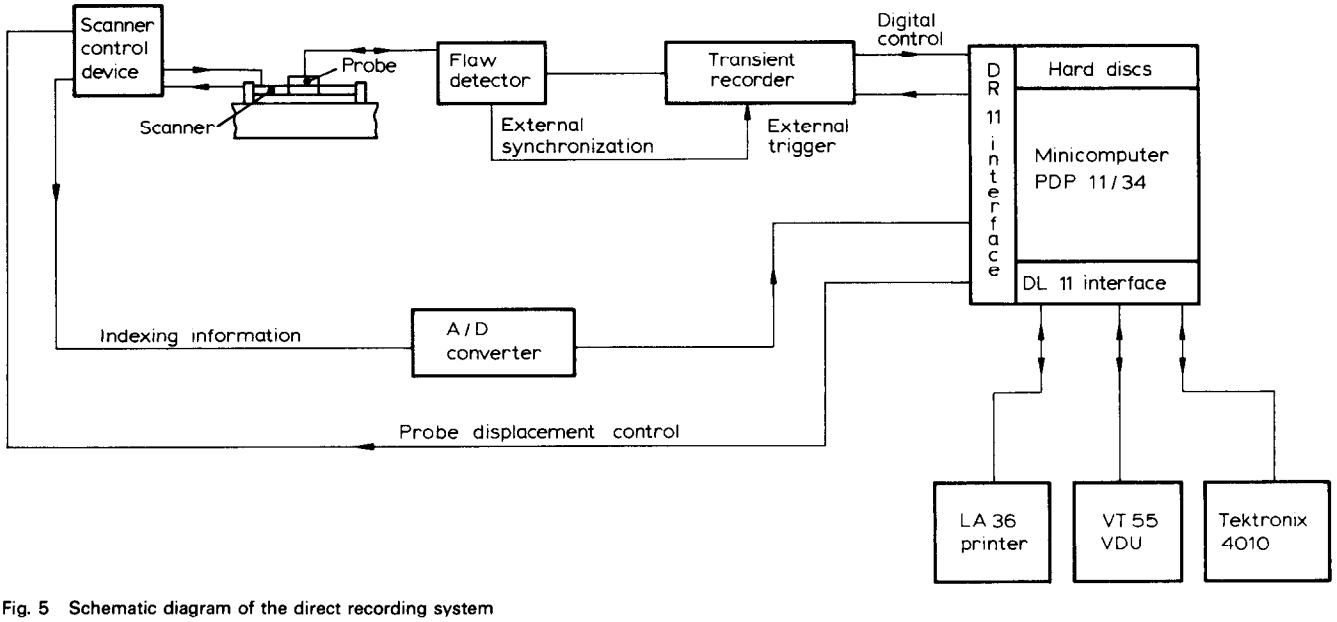

Fig. 5 Schematic diagram of the direct recording system

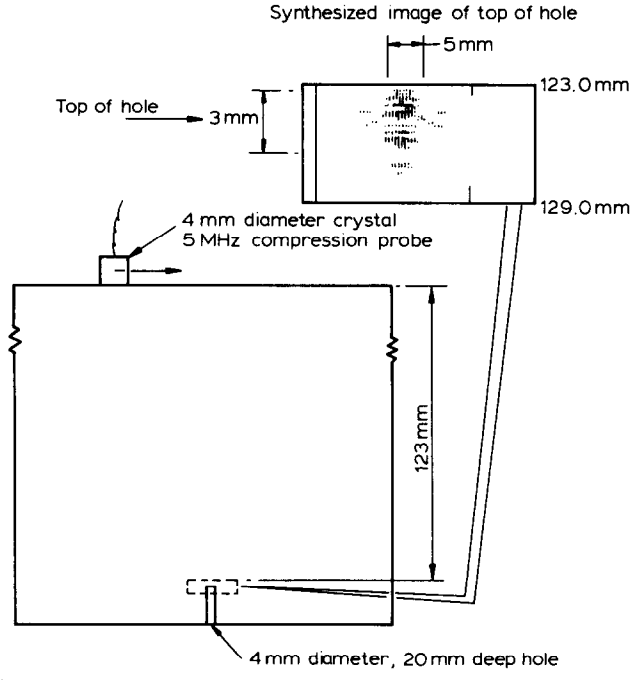

Fig. 6 SAFT analysis

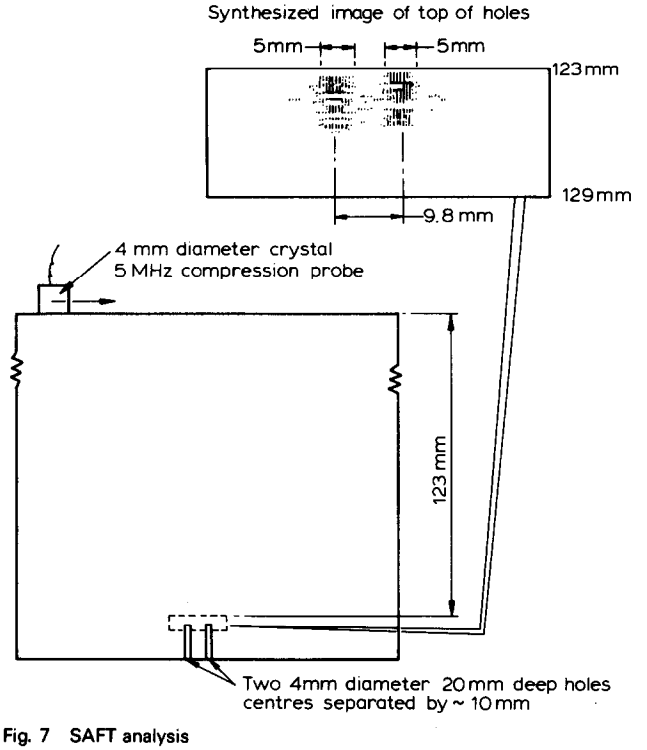

Fig. 7 SAFT analysis

point at which the point spread function decays to zero in the longitudinal direction, then the longitudinal resolution is $pc/4$, that is, one quarter the pulse length.

Experimental results

A limited number of experiments were performed to check the validity of the above resolutions. Fig. 5 gives a schematic diagram of the equipment used in the experiments. A 4 mm diameter crystal, 5 MHz compression probe was used to generate the wide-angle beam necessary for SAFT processing. Movement of the probe in increments as small as 0.1 mm over the surface of the component was achieved using an x-y scanner based on stepper motors. The rf echoes from the probe were fed, through a conventional ultrasonic flaw detector, into a fast transient recorder where they were digitized and stored in the machine's 4096 word memory. Signals captured by the transient recorder were then transferred to a PDP 11/34 computer with hard disc stores where SAFT analysis was performed on the collected data.

To obtain experimental values for SAFT's resolution, aluminium blocks containing flat-bottomed holes were fabricated to the dimensions shown in Figs 6–8. Using the scanner and probe described above, data were collected in a line scan directly above the centre lines of the holes. Rf echoes were recorded every 0.5 mm ($\lambda/2$) along the scan length, thus avoiding spatial aliasing of the reconstructed images, and some signal averaging was performed to improve the signal-to-noise ratio of the echoes. The SAFT algorithm was then applied to the collected data.

The result of applying SAFT to the data collected is shown in Figs 6–8, which contain grey scale B-scans of the synthesized data. The grey scale B-scan is generated on a Tektronix 4010 graphics storage scope. This scope has a screen with 1000 × 780 addressable points. To map a coarse version of $I(r')$, a 3 × 3 matrix of points is associated with each r' in the correct relative position on the screen and five types of matrix are defined containing 0, 1, 2, 4 and 9 printed points. Five levels are then defined within the dynamic range of $I(r')$; usually these levels are calculated by dividing the dynamic range by five to determine the increment between each level, the first level being set equal to this increment. Each of these levels is then associated with one of the matrices described above: usually the levels corresponding to larger values of I are associated with a larger number of matrix points. In this way a coarse grey scale B-scan can be produced. It can be seen from Figs 6–8 that the holes are easily resolved and that after subtracting the 4 mm hole diameter the expected transverse resolution of about 1 mm ($a/4$) is achieved. This experimental transverse resolution is

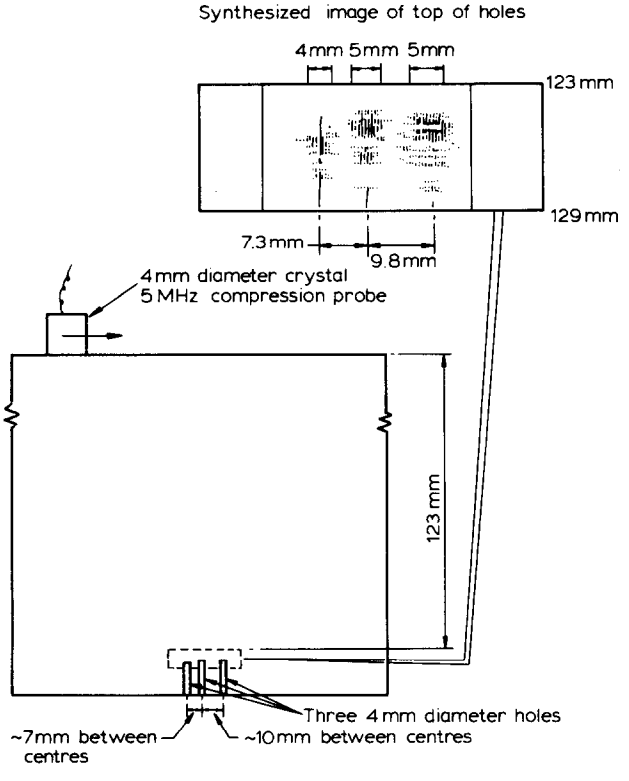

Fig. 8 SAFT analysis

further verified in Figs 9–11 where the maximum amplitude of the synthesized echoes is plotted against distance along the line scan over the holes. The theoretical longitudinal resolution can also be confirmed with reference to Figs 6 and 12; Fig. 12 contains a plot of the pulse shape of the data on which the SAFT algorithms were applied. It can be seen that the top of the holes are resolved to about $pc/4$, that is 1.5 mm.

Discussion and summary

To obtain the theoretical results above, a number of assumptions were made, the most obvious being the far-field assumption; however, it is worthwhile remarking on some of the other assumptions, namely beam profile and pulse shape. It was tacitly assumed in the text that the beam profile was constant over the beam width. This is clearly not the case in practice, in fact a $\sin(x)/x$ function would be more appropriate. If this beam profile term had been included, (11) would take the form

$$X_T(R, |r'|, \omega/c) = \int \frac{f(v)\, b(r_s, |r'|) \exp(-i\omega v)\, dr_s}{|r'|^2}$$

where $b(r_s|r'|)$ is the term that describes the beam profile as a function of r_s and the depth of imaging $|r'|$. Similarly for (17)

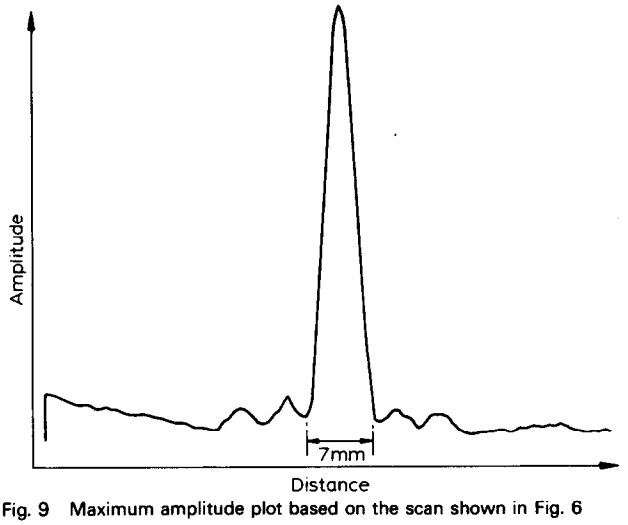

Fig. 9 Maximum amplitude plot based on the scan shown in Fig. 6

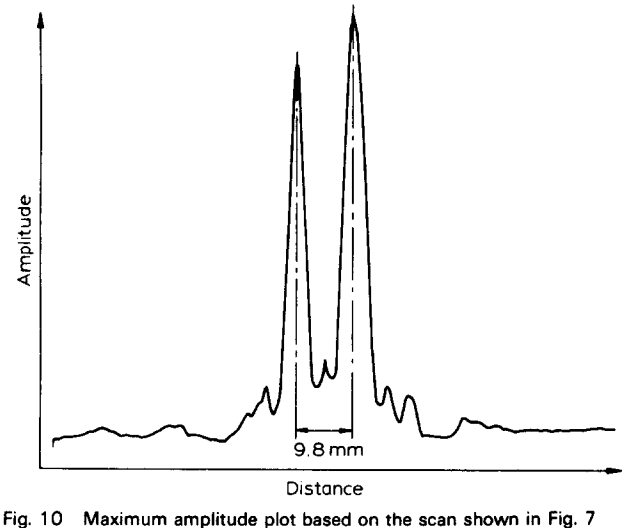

Fig. 10 Maximum amplitude plot based on the scan shown in Fig. 7

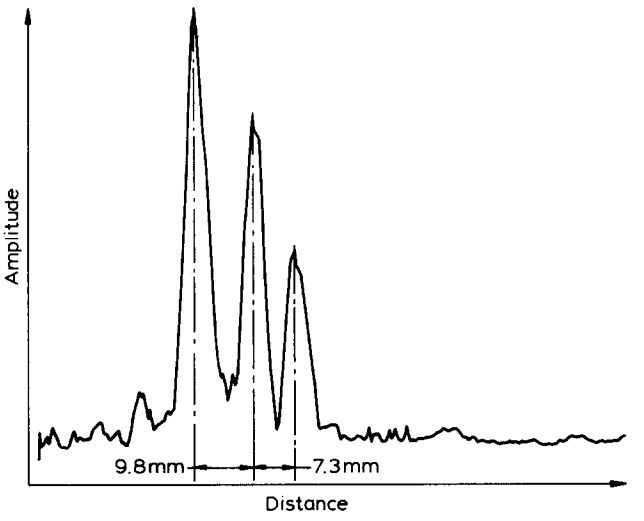

Fig. 11 Maximum amplitude plot based on the scan shown in Fig. 8

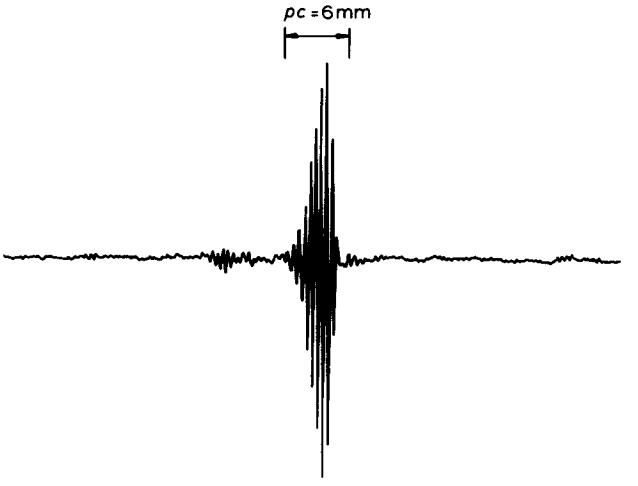

Fig. 12 Pulse shape

$$X_L(R, |r'|, \omega/c) = \int \frac{f(y)\, b(r_s|r'|) \exp(-i\omega y)\, dr_s}{|r'|^2}$$

Clearly the beam profile has no effect on the longitudinal resolution since none of the terms in the above integral depend upon the integration variable (apart from the beam profile term) and all the remaining integration does is modify the amplitude of the point spread function in the longitudinal direction. However, the situation regarding the transverse resolution is not so straightforward.

An indication of the effect of the beam spread term on the transverse resolution can be given by calculating X for the simple case of a beam profile which decreases linearly to zero either side of its centre line. For this case the transverse resolution is degraded by a factor of 2 to $a/2$. Similar comments also apply to pulse shape since the f term in the above equations behaves, in the most important aspects, like the b term. Therefore the comparison of theory with experiment above should be viewed with this in mind.

However, even with the above assumptions there is reasonable agreement between theory and the limited number of experiments performed and therefore the calculated transverse resolution of $a/4$ and longitudinal resolution of $pc/4$ appears to be correct. Further work could be aimed at a more extensive experimental investigation of the SAFT resolution combined with a

more detailed theoretical analysis of expected SAFT images from various types of defect.

Acknowledgement

The work was carried out in the NE Region Scientific Services Department and the paper is published by permission of the Director General, NE Region, CEGB.

References

1 **Johnson, J.** EG & G Idaho Inc., Idaho Falls, Idaho, (1981)
2 **Frederick et al.,** Conference on the Periodic Inspection of Pressure Vessels, Institute of Mechanical Engineers, (1979)
3 **Born, M. and Wolf, E.** Principles of Optics, Pergamon Press, (1975)
4 **Sherwin, C.W., et al.,** Some Early Developments in Synthetic Aperture Radar Systems, IRE Trans MIL-6. (1962) 111–115
5 **Flaherty, J.J. et al.,** Synthetic Aperture Ultrasonic Imaging Systems US Patent No. 3548642, (1967)
6 **Krautkramer, J., Krautkramer, H.** Ultrasonic Testing of Materials, Springer Verlag (1969)